ACS OMEGA

http://pubs.acs.org/journal/acsodf

Article

Bandgap Modulation of Cs_2AgInX_6 (X = Cl and Br) Double Perovskite Nano- and Microcrystals via Cu^{2+} Doping

Kangyong Kim,[§] Hyeonjung Kim,[§] and Jongnam Park*

Cite This: *ACS Omega* 2021, 6, 26952−26958

Read Online

ACCESS | Metrics & More | Article Recommendations | Supporting Information

ABSTRACT: Recently, the double perovskite $Cs_2AgInCl_6$, which has high stability and low toxicity, has been proposed as a potential alternative to Pb-based perovskites. However, the calculated parity-allowed transition bandgap of $Cs_2AgInCl_6$ is 4.25 eV; this wide bandgap makes it difficult to use as an efficient solar absorber. In this study, we explored the effect of Cu doping on the optical properties of $Cs_2AgInCl_6$ double perovskite nano- and microcrystals (MCs), particularly in its changes of absorption profile from the ultraviolet (UV) to near-infrared (NIR) region. Undoped $Cs_2AgInCl_6$ showed the expected wide bandgap absorbance, but the Cu-doped sample showed a new sharp absorption peak at 419 nm and broad absorption bands near 930 nm, indicating bandgap reduction. Electron paramagnetic resonance (EPR) spectroscopy demonstrated that this bandgap reduction effect was due to the Cu doping in the double perovskite and confirmed that the Cu^{2+} paramagnetic centers were located on the surface of the nanocrystals (NCs) and at the center of the perovskite octahedrons ($g_{\parallel} > g_{\perp} > g_e$). Finally, we synthesized Cu-doped $Cs_2AgInCl_6$ MCs and observed results similar to those of the NCs, showing that the application range could be expanded to multidimensions.

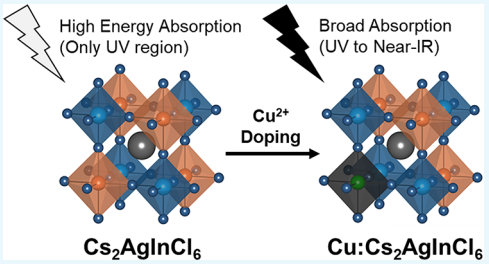

INTRODUCTION

As the demand for sustainable energy production has increased significantly, studies of materials with high photoconversion efficiency are being actively conducted. Among them, organic−inorganic lead halide perovskites ($APbX_3$; A: monovalent cation, $CH_3NH_3^+$, $CH(NH_2)_2^+$, and Cs^+; X: halide anion, Cl^-, Br^-, and I^-) are currently the most attractive materials because of their facile solution processability and excellent optoelectronic properties, such as high absorption coefficients, low exciton binding energy, and high carrier mobility. For this reason, perovskites have been widely studied in various shapes and compositions from quantum-confined nanocrystals (NCs) to polycrystalline thin films.[1−6] In particular, iodine-based $APbI_3$ materials have been applied as highly efficient light absorbers because of their narrow bandgap and wide-range absorption.[7,8] Nevertheless, the high toxicity of Pb and the intrinsic chemical instability of these materials, which are easily converted into the orthorhombic δ phase, make them difficult to use in practical applications.[9−12] Therefore, the search for non-toxic and stable perovskite materials has become important for the development of next-generation photovoltaics.

To develop Pb-free metal halide perovskites, isovalent substitutes for Pb^{2+}, such as Sn^{2+} or Ge^{2+}, have been considered. However, these species are easily oxidized to tetravalent ions (Sn^{4+} or Ge^{4+}) under ambient conditions and exhibit self-doping within the crystals as a p-type dopant, negatively affecting their photovoltaic properties.[13−16] Recently, double perovskites ($A_2B'B''X_6$, elpasolite), in which the divalent sites are replaced with a combination of monovalent (B′) and trivalent ions (B″), have been synthesized and demonstrated enhanced air and moisture stability.[17−21] Various cation compositions can be used to synthesize double perovskites, among which Cs_2AgBiX_6 (X = Cl^-, Br^-, and I^-) has been proposed as a non-toxic, highly stable candidate.[19,21−23] However, these exhibited low absorption coefficients and low photoluminescence (PL) quantum yields due to the limitations of materials with indirect bandgaps. Therefore, the direct bandgap double perovskite, $Cs_2AgInCl_6$, has been studied in various forms, from nanoparticles to bulk single crystals.[20,24]

Since the first colloidal synthesis of $Cs_2AgInCl_6$ NCs was reported in 2018,[24] various studies have analyzed the physical and optical properties of these materials.[25−28,35] According to the results of density functional theory calculations and bandgap analysis of the synthesized NCs, the parity-allowed transition bandgap of $Cs_2AgInCl_6$ was calculated to be 4.25 eV;[27] this wide bandgap makes it difficult to use as an efficient light absorber. To increase its applicability, several authors have reported the strategy of modifying the optical properties of $Cs_2AgInCl_6$ via doping with heteroelements. Locardi *et al.* suggested an efficient colloidal route to synthesize $Cs_2AgInCl_6$

Received: June 23, 2021
Accepted: September 30, 2021
Published: October 8, 2021

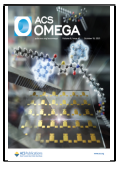

https://doi.org/10.1021/acsomega.1c03290
ACS Omega 2021, 6, 26952−26958

NCs and also confirmed the possibility of emission tuning via the orange emission of Mn-doped $Cs_2AgInCl_6$ NCs.[24] Additionally, Lee *et al.* synthesized lanthanide-doped $Cs_2AgInCl_6$ NCs and observed their characteristic f−f transition emission in the near-infrared (NIR) region (996 nm for Yb^{3+} and 1537 nm for Er^{3+}).[26] Although various doping approaches have been studied, these studies have focused on changes in the emission properties due to internal energy transfer. Some studies have dealt with reducing the bandgap through doping to achieve extended absorption, but these presented drawbacks. $Cs_2(Ag_{1-a}Bi_{1-b})Tl_xBr_6$[29] and Cu^{2+}-doped $Cs_2AgSbCl_6$ have shown effective bandgap reduction,[30] but these materials contain Tl and Sb, which are as toxic as Pb, and are limited to bulk crystals. To solve this problem, non-toxic lead-free double perovskite NCs such as $Cs_2AgInCl_6$, $Cs_2AgBiBr_6$, and $Cs_2NaBiCl_6$ were successfully doped with various elements including Cu^{2+}, Ag^+, Mn^{2+}, or Eu^{3+} demonstrating the change of optical properties.[35−37]

In this work, we synthesized Cu-doped $Cs_2AgInCl_6$ (Cu:$Cs_2AgInCl_6$) NCs and microcrystals (MCs), which are based on earth-abundant and non-toxic elements, to achieve extended absorption. We analyzed the effect of Cu addition on the absorption profile and verified that the observed changes were not due to the generation of byproducts during colloidal synthesis. The bandgap of the Cu:$Cs_2AgInCl_6$ NCs was 2.56 eV, which represented a significant reduction compared to that of undoped $Cs_2AgInCl_6$ NCs, and the broad absorption features near the NIR region due to the Cu defect states enabled extended absorption for high-efficiency light absorber applications. The bandgap changes due to Cu doping were further modified through halide exchange at room temperature. Moreover, synthesis of Cu-doped MCs revealed that the doping effects in the NCs could be observed even in the bulk case, further expanding the application scope.

EXPERIMENTAL SECTION

Materials. Cesium carbonate (Cs_2CO_3, 99.9%), silver acetate (Ag(OAc), 99%), indium(III) acetate ($In(OAc)_3$, 99.99% trace metal basis), copper(II) acetate ($Cu(OAc)_2$, 99.99% trace metal basis), cesium chloride (CsCl, 99.9%), silver chloride (AgCl, 99.999% trace metal basis), indium(III) chloride ($InCl_3$, 99.999% trace metal basis), copper(II) chloride dihydrate ($CuCl_2{\cdot}2H_2O$, 99.0%), oleic acid (OA, 90%), oleylamine (OAm, 70%), benzoyl bromide (Bz-Br, 97%), benzoyl chloride (Bz-Cl, 99%), diphenyl ether (DPE, 99%), hydrochloric acid (HCl, 37%), hexane (anhydrous, 95%), acetone (99.5%), and 2-propanol (99.5%) were obtained from Sigma-Aldrich. All chemicals were used as received without further purification.

Preparation of Cesium Oleate (Cs-OA). A 0.5 M Cs-OA solution was prepared by loading 0.815 g of Cs_2CO_3 (2.5 mmol) and 10.0 mL of OA into a 50 mL round-bottom three-neck flask. The flask was degassed and slowly heated to 120 °C. After 30 min of degassing, the temperature was raised to 150 °C, and the flask was maintained at this temperature for 2 h under an inert atmosphere of Ar. The solution was cooled to room temperature with Ar purging and stored in a vial.

Synthesis of $Cs_2AgInCl_6$ and Cu:$Cs_2AgInCl_6$ NCs. $Cs_2AgInCl_6$ NCs were synthesized following the method developed by Locardi *et al.*[24] First, 0.04 g of Ag(OAc) (0.24 mmol), 0.073 g of $In(OAc)_3$ (0.25 mmol), 0.5 mL of OAm, 1 mL of the Cs-OA solution, and 4 mL of DPE were loaded into a 50 mL round-bottom three-neck flask. The Cu:$Cs_2AgInCl_6$ NCs were obtained by adding $Cu(OAc)_2$ to the precursor mixture. The flask was heated to 40 °C with degassing. After 30 min of degassing, the temperature reached 105 °C (ramping rate: 10 °C/min). When the temperature was reached to the point, 0.2 mL of Bz-Cl mixed with 0.5 mL of degassed DPE was rapidly injected into the solution. The reaction was quenched after growth by cooling in an ice-water bath. The product solution was centrifuged at 7830 rpm for 10 min, and the precipitates were redispersed in hexane. For purification of the NCs, a small amount of acetone was added to precipitate the NCs followed by centrifugation and decantation of the supernatant. The precipitates were redispersed in hexane.

Synthesis of $Cs_2AgInCl_6$ and Cu:$Cs_2AgInCl_6$ MCs. An amount of 0.221 g of $InCl_3$ (1.0 mmol), 0.129 g of AgCl (0.9 mmol), and 10.0 mL of 10 M HCl aqueous solution were loaded into a 70 mL vial with a magnetic stir bar. The vial was heated with vigorous stirring on a hotplate at 120 °C. After the complete dissolution of all components, 0.337 g of CsCl (2.0 mmol) was poured into the vial. $Cs_2AgInCl_6$ MCs were immediately observed. The Cu:$Cs_2AgInCl_6$ MCs were obtained by adding a known amount of $CuCl_2{\cdot}2H_2O$ along with CsCl. The MCs were then filtered, washed with 2-propanol, and dried overnight.

Optical Properties. The absorption spectra were measured using a Shimadzu UV-1800 ultraviolet (UV)−visible (vis)−NIR spectrometer. The PL spectra were taken with an Agilent fluorescence spectrophotometer (λ_{ex} = 310 nm). The diffuse reflectance spectra were measured using an Agilent Cary 5000 spectrometer.

Dynamic Light Scattering. Dynamic light scattering (DLS) measurements were performed on a Malvern Instruments Zetasizer Nano-ZS90 at 25 °C.

Electron Microscopy. Transmission electron microscopy (TEM) images were obtained with a JEOL JEM-2100 microscope with an acceleration voltage of 200 kV using gold grids (Ted Pella, USA). Samples for TEM imaging were prepared by dropping a diluted hexane solution of the NCs onto the grids. The solvent was evaporated prior to imaging. The MCs were investigated using field emission electron scanning microscopy (FE-SEM, Hitachi, SU8220).

X-ray Powder Diffraction. X-ray powder diffraction (XRD) was carried out with a Rigaku D/MAX2500V/PC X-ray diffractometer operated at 40 kV/200 mA using a Cu Kα line (λ = 1.5405 Å). The purified samples were dried fully before analysis.

Electron Paramagnetic Resonance Spectroscopy. All electron paramagnetic resonance spectroscopy (EPR) measurements were performed at the Western Seoul Center, Korea Basic Science Institute (KBSI) in Seoul, Korea. The CW X-band (9.6 GHz) EPR spectra were collected using a Bruker EMX plus 6/1 spectrometer equipped with an Oxford Instrument ESR900 liquid He cryostat using an Oxford ITC 503 temperature controller. All spectra were collected with the following experimental parameters: microwave frequency, 9.6 GHz; microwave power, 1 mW; modulation amplitude, 10 G; time constant, 20.48 ms; and temperature, 20 K.

X-ray Photoelectron Spectroscopy. X-ray photoelectron spectroscopy (XPS) was performed using a Thermo Scientific K-Alpha spectrometer. The powder obtained through lyophilization of the purified NC solution was used as a sample for XPS analysis.

https://doi.org/10.1021/acsomega.1c03290
ACS Omega 2021, 6, 26952−26958

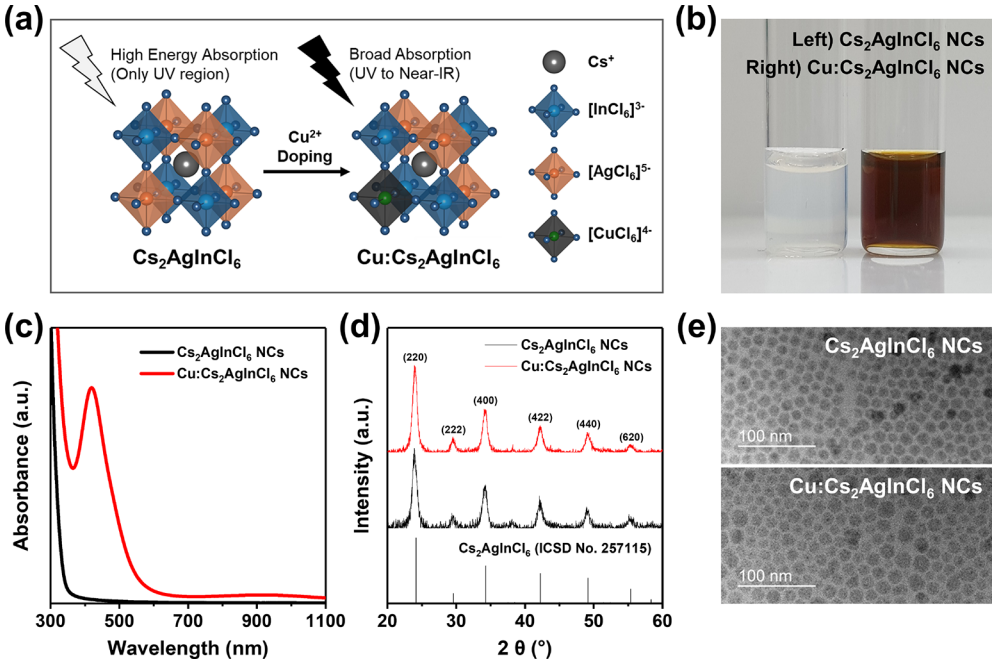

Figure 1. Observation of the effect of Cu doping on $Cs_2AgInCl_6$ NCs. (a) Schematic illustration of the bandgap reduction in Cu-doped $Cs_2AgInCl_6$ ($Cu:Cs_2AgInCl_6$). (b) Photo of $Cs_2AgInCl_6$ and $Cu:Cs_2AgInCl_6$ NCs solutions. (c) UV−vis−NIR absorption spectra. (d) XRD characterization. (e) TEM analysis results for the $Cs_2AgInCl_6$ and $Cu:Cs_2AgInCl_6$ NCs. Photograph courtesy of "Kangyong Kim". Copyright 2021.

RESULTS AND DISCUSSION

For the colloidal hot-injection synthesis of $Cs_2AgInCl_6$ double perovskite NCs, we followed a previously reported method.[24] To synthesize $Cu:Cs_2AgInCl_6$ NCs, $Cu(OAc)_2$ was added to the precursor mixture. As a result, a dark brown solution was obtained immediately after the injection of Bz-Cl when $Cu(OAc)_2$ was added. Undoped $Cs_2AgInCl_6$ is a white solid with a wide bandgap. We hypothesized that this color change was due to a bandgap shift caused by Cu doping. The schematic illustration in Figure 1a illustrates our hypothesis regarding the bandgap shift and extended absorption due to Cu doping.

Figure 1b is a photograph of solutions of undoped $Cs_2AgInCl_6$ and $Cu:Cs_2AgInCl_6$ NCs. We conducted additional analyses to verify that the bandgap shift was the result of Cu doping rather than other impurities that could be generated during the colloidal synthesis process. UV−vis−NIR absorption spectrum analysis indicated that undoped $Cs_2AgInCl_6$ exhibited the expected wide bandgap absorbance, but the Cu-doped sample showed a new sharp absorption peak at 419 nm (Figure 1c). This was similar to the typical absorption spectrum featuring a sharp absorption peak observed after Bi doping in the previously reported $Cs_2AgIn_xBi_{1-x}Cl_6$ NCs.[27] In addition, when the NIR region (700−1100 nm) of the spectrum was magnified (Figure S1), the absorption was found to begin with a broad absorption band near 930 nm (1.33 eV), which was assignable to the $^2E_g \rightarrow {}^2T_{2g}$ transition of Cu^{2+}. Thus, after the addition of Cu, the limited absorption in the high-energy region (~400 nm) was extended to the NIR region (~1100 nm). Figure 1d shows the results of XRD analysis, demonstrating that the patterns of the undoped and Cu-doped samples coincided with the XRD peaks of bulk $Cs_2AgInCl_6$ (ICSD no. 257115) and that no other impurities were observed. Figure S2 shows the $Cu:Cs_2AgInCl_6$ NCs powder used for XRD analysis, which was obtained by lyophilization after washing. These results suggested that the observed changes in the absorption were not due to byproducts produced during colloidal synthesis. In addition, as shown in Figure S3, the highly intense (220) peak of the $Cu:Cs_2AgInCl_6$ NCs was shifted slightly toward the higher angle region due to the decrease in the average lattice parameter as the small Cu^{2+} ions (ionic radius of Cu^{2+}: 87 pm, Ag^+: 129 pm, and In^{3+}: 94 pm) were doped into the lattice. Figure 1e and Figure S4 show the results of TEM analysis, which reveal that both the undoped and $Cu:Cs_2AgInCl_6$ NCs were approximately about 17 nm ± 2 nm in size.

In order to more closely analyze the effect of Cu doping on $Cu:Cs_2AgInCl_6$, the changes in the absorption spectrum were observed for samples produced using different amounts of Cu. The spectral data in Figure 2b, which is a magnification of the region in the red box region in Figure 2a, showed that the intensity of the sharp absorption peak at 419 nm and the broad absorption band in the NIR region increased as the Cu/In ratio in the precursor mixture was increased to from 0.04 to 0.08 and 0.4. In the case of Cu/In = 0.4 containing excess Cu, unreacted Cu-oleate was detected in the decanted supernatant (no nanoparticles included) separated after the reaction (Figure S5). These results demonstrate that the change in the absorption spectrum was due to Cu and that there is a limit to the amount of Cu that can be doped (doping limit) into the $Cs_2AgInCl_6$ NCs. Therefore, subsequent synthesis was carried out under the conditions of Cu/In = 0.2 below the doping limit. To determine the actual amount of Cu-doped into the particles, elemental analysis was conducted via XPS and inductively coupled plasma optical emission spectroscopy (ICP-OES) of the purified sample, and the Cu-doped NCs were found to contain 1.7 atomic% Cu relative to the total elements (Table S1).

In addition, EPR analysis was performed to analyze the presence or absence of Cu doping and the environment of Cu in the lattice. EPR analysis has been used as a sensitive spectroscopic technique to determine the local coordination of

https://doi.org/10.1021/acsomega.1c03290
ACS Omega 2021, 6, 26952−26958

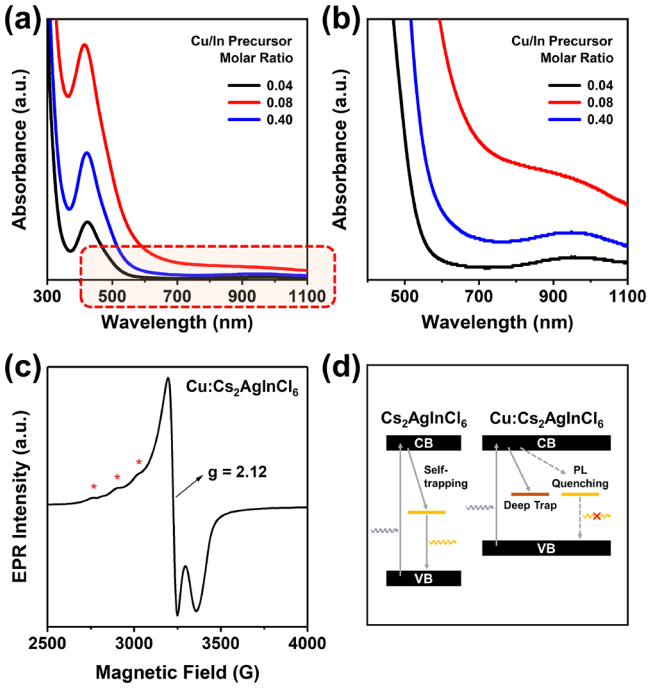

Figure 2. (a) UV−vis−NIR absorption spectra of Cu:$Cs_2AgInCl_6$ NCs with different amounts of Cu (Cu/In precursor molar ratio = 0.04, 0.08, and 0.40). (b) Magnified UV−vis−NIR absorption spectra (region in the red box in (a)). (c) EPR spectrum of Cu:$Cs_2AgInCl_6$ NCs in solution. (d) Band diagram of $Cs_2AgInCl_6$ and Cu:$Cs_2AgInCl_6$ NCs.

doped paramagnetic centers.[31−33] In particular, it has been used extensively to analyze the doping environment of Mn^{2+} in perovskites. The Cu^{2+} ion is also a useful probe, as it has effective electron spin S of 1/2 and a nuclear spin I of 3/2. Figure 2c shows the results of the X-band (9.6 GHz) low-temperature (20 K) EPR analysis of the Cu:$Cs_2AgInCl_6$ NCs (Cu/In = 0.2). Both an isotropic signal (an intense and broad spectrum) and a relatively weak anisotropic signal (marked with *, a structured spectrum) originating from Cu^{2+} were observed. This indicates that dipolar interactions between Cu^{2+} ions occur on the surface of the nanoparticles and smear the hyperfine interaction and that the ratio of internally doped Cu^{2+} is relatively small. In addition, considering the fact that $g_{\parallel} > g_{\perp} > g_e$ (g_e = 2.0023), it can be assumed that the internally doped Cu^{2+} is located at distorted octahedral sites of the perovskite. The above results confirmed that Cu was doped into the $Cs_2AgInCl_6$ NCs. Based on the electronegativities of the constituent elements (Cs:0.79, Ag:1.93, Cu:1.90, and In:1.78), it was expected that the internally doped Cu was most likely doped in the form of $[CuCl_6]^{4-}$ at the $[AgCl_6]^{5-}$ site. Next, we calculated the bandgap from the corresponding Tauc plots to determine the effect of Cu doping on the bandgap shift and extended absorption (Figure S6). The optical bandgap of the undoped $Cs_2AgInCl_6$ was 4.21 eV, which is similar to the previously reported parity-allowed transition of $Cs_2AgInCl_6$ NCs.[27] In contrast, the bandgap of the Cu:$Cs_2AgInCl_6$ NCs was 2.56 eV, which represented a significant bandgap reduction compared to undoped NCs. According to the previous studies, the bandgap reduction observed in Cu:$Cs_2AgInCl_6$ NCs was the result of shifting the Ag 4d-derived valence band (VB) to a higher energy level due to the overlapping of Cu 3d orbitals with Ag 4d orbitals.[35,38]

Figure S7 shows the PL spectra of $Cs_2AgInCl_6$ and Cu:$Cs_2AgInCl_6$ NCs. The broad emission of $Cs_2AgInCl_6$ centered at 525 nm is related to self-trapped excitons (STEs) that arose from the strong Jahn−Teller distortion of the $[AgCl_6]$ octahedron.[39]

However, no luminescence was observed in the Cu-doped sample, and this PL quenching is presumed to be the result of non-radiative recombination triggered by deep trap states resulting from Ag vacancies generated to maintain the charge neutrality. This phenomenon was also observed similarly in Cu-doped TiO_2 nanoparticles, which showed a decrease of the STEs' emission by deep trap states.[40] Figure 2d is a band diagram showing the change in the bandgap and emission characteristics of $Cs_2AgInCl_6$ due to Cu doping.

Additionally, to optimize the synthesis conditions and optical character of the Cu:$Cs_2AgInCl_6$ NCs, we adjusted the growth time after nucleation. The NCs were grown for 5, 30, or 60 s after injecting Bz-Cl, and the resulting size distributions were analyzed using DLS (Figure 3a). As the growth time

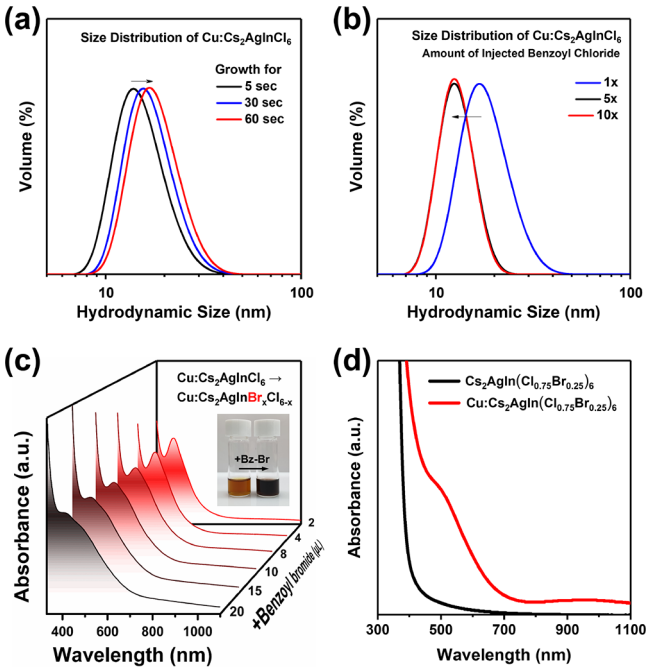

Figure 3. (a) DLS results for Cu:$Cs_2AgInCl_6$ NCs with different growth times (5, 30, or 60 s). (b) DLS results for Cu:$Cs_2AgInCl_6$ NCs with different amounts of injected Bz-Cl (1×, 5×, or 10×). (c) Changes in absorbance during anion exchange. (d) Absorbance of $Cs_2AgIn(Cl_{0.75}Br_{0.25})_6$ and Cu:$Cs_2AgIn(Cl_{0.75}Br_{0.25})_6$ NCs. Photograph courtesy of "Kangyong Kim". Copyright 2021.

increased, the average hydrodynamic size gradually increased from 15.44 to 18.43 nm, and the corresponding decrease in the polydispersity index (PDI) from 0.342 to 0.123 showed an improvement in uniformity (Table S2). In a previous study by Imran *et al.*, it was reported that using a single halide source, such as benzoyl halide, as an injection source, could easily create an excess halide condition and fine-tune the size distribution of perovskite NCs.[34] Therefore, to achieve more uniform nucleation and growth, the changes in the size distribution was measured while varying the amount of injected Bz-Cl under the conditions of 60 s growth time. DLS analysis showed that the average particle size decreased and the overall size distribution became more uniform as the

https://doi.org/10.1021/acsomega.1c03290
ACS Omega 2021, 6, 26952−26958

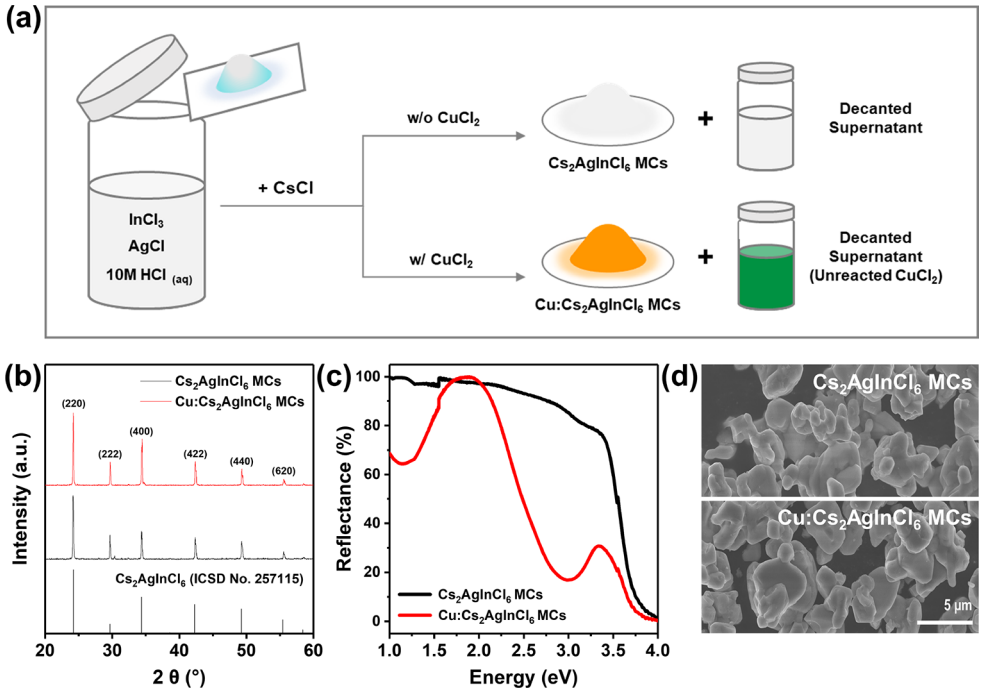

Figure 4. Results for the synthesized Cu:$Cs_2AgInCl_6$ MCs. (a) Schematic illustration of the synthesis of $Cs_2AgInCl_6$ and Cu:$Cs_2AgInCl_6$ MCs. (b) XRD characterization. (c) Diffuse reflectance spectra. (d) SEM analysis results of $Cs_2AgInCl_6$ and Cu:$Cs_2AgInCl_6$ MCs.

amount of halide source was increased (Figure 3b). The reaction conditions were optimized for the synthesis of monodisperse nanoparticles, and further experiments were carried out to determine whether additional absorption extension through halide exchange was possible for the Cu-doped double perovskites.

Figure 3c shows the changes in the absorbance of the halide-exchanged Cu:$Cs_2AgInBr_xCl_{6-x}$ obtained by adding (2−20 μL) Bz-Br to the synthesized Cu:$Cs_2AgInCl_6$ solution at room temperature. As more Bz-Br was added, the sharp absorption peak at 419 nm gradually red-shifted and broadened due to halide exchange (Figure 3c and Figure S8), which also produced a visual color change (Figure 3c, inset photograph). Furthermore, to confirm that the change was caused by anion exchange, the results were compared with those for Cu-doped mixed halide double perovskites synthesized by adjusting the ratio between the injected halide sources. Figure 3d shows the absorption spectra of $Cs_2AgIn(Cl_{0.25}Br_{0.75})_6$ and Cu:$Cs_2AgIn(Cl_{0.25}B_{0.75})_6$ NCs synthesized by injecting a halide mixture (Bz-Br:Bz-Cl = 1:3). The effect of Cu doping was also observed in the mixed halide composition, which is consistent with the observed changes after anion exchange. Thus, even in Cu:$Cs_2AgInCl_6$, additional bandgap tuning is possible through changing the halide composition.

Moreover, we compared the doping effects observed in Cu:$Cs_2AgInCl_6$ NCs to those in Cu:$Cs_2AgInCl_6$ MCs to expand its application scope. Figure 4a shows a schematic illustration of the synthesis process and the results for undoped $Cs_2AgInCl_6$ and Cu:$Cs_2AgInCl_6$ MCs. When CsCl was mixed with $CuCl_2$ for Cu doping, a dark orange powder immediately precipitated. Figure S9 is a photograph of the synthesized $Cs_2AgInCl_6$ MCs and Cu:$Cs_2AgInCl_6$ MCs and shows the distinct color difference due to the bandgap reduction. In addition, when $CuCl_2$ was used, the decanted supernatant was dark green. This is the color of the coordination complex formed by Cu ions in the presence of a high concentration of [Cl^-], indicating that unreacted Cu above the doping limit was present.

Figure 4b shows the XRD patterns of the undoped and Cu-doped MCs, which were characterized as $Cs_2AgInCl_6$ without impurities. The diffuse reflectance spectra of the MCs in Figure 4c and the Kubelka−Munk function ($F(R) = (1 - R)^2/2R$) in Figure S10 indicated that they exhibited doping effects similar to those observed in the Cu:$Cs_2AgInCl_6$ NCs. The Cu-doped NCs were darker than the MCs (Figure S9), presumably due to Urbach tails caused by defects, which can easily be generated on the nanoparticle surface. In addition, the synthesized MCs were characterized using SEM, but no macroscopic differences were observed between the MCs with or without Cu doping (Figure 4d and Figure S11). The SEM−energy-dispersive X-ray spectrometry (EDS) results summarized in Table S3 indicated that Cu:$Cs_2AgInCl_6$ MCs synthesized with Cu/In = 0.2 contained 2.05 atomic% of Cu. The consistency between the experimental results for the NCs and MCs clearly demonstrated that the Cu doping effect was not due to byproducts produced during the colloidal synthesis of the nanoparticles and the method could be extended to bulk crystals.

CONCLUSIONS

We investigated the effect of Cu^{2+} doping on the optical properties of $Cs_2AgInCl_6$ double perovskite NCs and MCs, especially the changes in the absorption spectra in the UV to NIR region. Undoped $Cs_2AgInCl_6$ has low toxicity and high stability, but its applications are limited owing to its wide bandgap. We added Cu^{2+} to the reaction precursor and observed a distinct change in color. This change was confirmed to be due to the bandgap reduction of $Cs_2AgInCl_6$. Furthermore, to confirm that the effect was caused by Cu^{2+} doping of the perovskite, several analyses were conducted. The EPR results clearly demonstrated that the Cu^{2+} paramagnetic centers were located on the surface of the NCs and at the

https://doi.org/10.1021/acsomega.1c03290
ACS Omega 2021, 6, 26952−26958

center of the perovskite octahedrons. We improved the size uniformity of Cu:$Cs_2AgInCl_6$ NCs by optimizing the reaction time and amount of halide precursors. In addition, we synthesized Cu:$Cs_2AgInBr_xCl_{6-x}$ NCs via anion exchange, resulting in the bandgap shift and the additional absorption extension even in the doped condition. Finally, we synthesized Cu:$Cs_2AgInCl_6$ MCs, which exhibited similar results to those of the NCs, and found that the series of changes induced by the addition of Cu were not due the generation of a byproduct during the colloidal synthesis of NCs, and the application range could be expanded to multidimensions. We believe that this Cu doping strategy will further enhance the applicability of double perovskites to photoelectric devices.

■ ASSOCIATED CONTENT

Supporting Information

The Supporting Information is available free of charge at https://pubs.acs.org/doi/10.1021/acsomega.1c03290.

Magnified absorption spectra of the $Cs_2AgInCl_6$ and Cu:$Cs_2AgInCl_6$ NCs; photograph of Cu:$Cs_2AgInCl_6$ NCs powder; magnified XRD patterns of $Cs_2AgInCl_6$ and Cu:$Cs_2AgInCl_6$ NCs; TEM images; photograph of the decanted supernatant; the absorption spectrum of the decanted supernatant; Tauc plots of the $Cs_2AgInCl_6$ and Cu:$Cs_2AgInCl_6$ NCs; the PL spectra of $Cs_2AgInCl_6$ and Cu:$Cs_2AgInCl_6$ NCs; the absorption spectra of the anion-exchanged Cu:$Cs_2AgInBr_xCl_{6-x}$ NCs; photograph of $Cs_2AgInCl_6$ and Cu:$Cs_2AgInCl_6$ MCs; the Kubelka–Munk function; SEM images; elemental analysis results (XPS and ICP-OES); DLS results; elemental analysis results (SEM-EDS) (PDF)

■ AUTHOR INFORMATION

Corresponding Author

Jongnam Park − *School of Energy and Chemical Engineering and Department of Biomedical Engineering, Ulsan National Institute of Science and Technology (UNIST), Ulsan 44919, Republic of Korea;* orcid.org/0000-0002-0954-0172; Email: jnpark@unist.ac.kr

Authors

Kangyong Kim − *School of Energy and Chemical Engineering, Ulsan National Institute of Science and Technology (UNIST), Ulsan 44919, Republic of Korea*

Hyeonjung Kim − *School of Energy and Chemical Engineering, Ulsan National Institute of Science and Technology (UNIST), Ulsan 44919, Republic of Korea;* orcid.org/0000-0002-9185-8269

Complete contact information is available at: https://pubs.acs.org/10.1021/acsomega.1c03290

Author Contributions

§K.K. and H.K. contributed equally to this work.

Notes

The authors declare no competing financial interest.

■ ACKNOWLEDGMENTS

This work was supported by the National Research Foundation (NRF) grants funded by the Korean government [no. NRF-2019R1A2C1010435], the Institutional Research Program of Korea Institute of Science and Technology (KIST) [no. 2E28070], and the Research Project Funded by U-K Brand (1.210047.01 and 1.210037.01) of UNIST.

■ REFERENCES

(1) Grätzel, M. The Light and Shade of Perovskite Solar Cells. *Nat. Mater.* **2014**, *13*, 838−842.

(2) Jeon, N. J.; Noh, J. H.; Yang, W. S.; Kim, Y. C.; Ryu, S.; Seo, J.; Seok, S. I. Compositional Engineering of Perovskite Materials for High-Performance Solar Cells. *Nature* **2015**, *517*, 476−480.

(3) Liu, M.; Johnston, M. B.; Snaith, H. J. Efficient Planar Heterojunction Perovskite Solar Cells by Vapour Deposition. *Nature* **2013**, *501*, 395−398.

(4) Protesescu, L.; Yakunin, S.; Bodnarchuk, M. I.; Krieg, F.; Caputo, R.; Hendon, C. H.; Yang, R. X.; Walsh, A.; Kovalenko, M. V. Nanocrystals of Cesium Lead Halide Perovskites ($CsPbX_3$, X = Cl, Br, and I): Novel Optoelectronic Materials Showing Bright Emission with Wide Color Gamut. *Nano Lett.* **2015**, *15*, 3692−3696.

(5) Protesescu, L.; Yakunin, S.; Kumar, S.; Bär, J.; Bertolotti, F.; Masciocchi, N.; Guagliardi, A.; Grotevent, M.; Shorubalko, I.; Bodnarchuk, M. I.; Shih, C.-J.; Kovalenko, M. V. Dismantling the "Red Wall" of Colloidal Perovskites: Highly Luminescent Formamidinium and Formamidinium−Cesium Lead Iodide Nanocrystals. *ACS Nano* **2017**, *11*, 3119−3134.

(6) Zhang, F.; Zhong, H.; Chen, C.; Wu, X.-G.; Hu, X.; Huang, H.; Han, J.; Zou, B.; Dong, Y. Brightly Luminescent and Color-Tunable Colloidal $CH_3NH_3PbX_3$ (X = Br, I, Cl) Quantum Dots: Potential Alternatives for Display Technology. *ACS Nano* **2015**, *9*, 4533−4542.

(7) Shin, S. S.; Yeom, E. J.; Yang, W. S.; Hur, S.; Kim, M. G.; Im, J.; Seo, J.; Noh, J. H.; Seok, S. I. Colloidally Prepared La-Doped $BaSnO_3$ Electrodes for Efficient, Photostable Perovskite Solar Cells. *Science* **2017**, *356*, 167−171.

(8) Turren-Cruz, S.-H.; Hagfeldt, A.; Saliba, M. Methylammonium-free, High-performance, and Stable Perovskite Solar Cells on a Planar Architecture. *Science* **2018**, *362*, 449−453.

(9) Dastidar, S.; Hawley, C. J.; Dillon, A. D.; Gutierrez-Perez, A. D.; Spanier, J. E.; Fafarman, A. T. Quantitative Phase-Change Thermodynamics and Metastability of Perovskite-Phase Cesium Lead Iodide. *J. Phys. Chem. Lett.* **2017**, *8*, 1278−1282.

(10) Juarez-Perez, E. J.; Hawash, Z.; Raga, S. R.; Ono, L. K.; Qi, Y. Thermal Degradation of $CH_3NH_3PbI_3$ Perovskite into NH_3 and CH_3I Gases Observed by Coupled Thermogravimetry−mass Spectrometry Analysis. *Energy Environ. Sci.* **2016**, *9*, 3406−3410.

(11) Marronnier, A.; Roma, G.; Boyer-Richard, S.; Pedesseau, L.; Jancu, J.-M.; Bonnassieux, Y.; Katan, C.; Stoumpos, C. C.; Kanatzidis, M. G.; Even, J. Anharmonicity and Disorder in the Black Phases of Cesium Lead Iodide Used for Stable Inorganic Perovskite Solar Cells. *ACS Nano* **2018**, *12*, 3477−3486.

(12) Zhao, B.; Jin, S.-F.; Huang, S.; Liu, N.; Ma, J.-Y.; Xue, D.-J.; Han, Q.; Ding, J.; Ge, Q.-Q.; Feng, Y.; Hu, J.-S. Thermodynamically Stable Orthorhombic γ-$CsPbI_3$ Thin Films for High-Performance Photovoltaics. *J. Am. Chem. Soc.* **2018**, *140*, 11716−11725.

(13) Takahashi, Y.; Hasegawa, H.; Takahashi, Y.; Inabe, T. Hall Mobility in Tin Iodide Perovskite $CH_3NH_3SnI_3$: Evidence for a Doped Semiconductor. *J. Solid State Chem.* **2013**, *205*, 39−43.

(14) Takahashi, Y.; Obara, R.; Lin, Z.-Z.; Takahashi, Y.; Naito, T.; Inabe, T.; Ishibashi, S.; Terakura, K. Charge-Transport in Tin-iodide Perovskite $CH_3NH_3SnI_3$: Origin of High Conductivity. *Dalton Trans.* **2011**, *40*, 5563−5568.

(15) Wu, X.; Song, W.; Li, Q.; Zhao, X.; He, D.; Quan, Z. Synthesis of Lead-Free $CsGeI_3$ Perovskite Colloidal Nanocrystals and Electron Beam-induced Transformations. *Chem. − Asian J.* **2018**, *13*, 1654−1659.

(16) Xu, P.; Chen, S.; Xiang, H.-J.; Gong, X.-G.; Wei, S.-H. Influence of Defects and Synthesis Conditions on the Photovoltaic Performance of Perovskite Semiconductor $CsSnI_3$. *Chem. Mater.* **2014**, *26*, 6068−6072.

(17) Filip, M. R.; Liu, X.; Miglio, A.; Hautier, G.; Giustino, F. Phase Diagrams and Stability of Lead-Free Halide Double Perovskites

$Cs_2BB'X_6$: B = Sb and Bi, B′ = Cu, Ag, and Au, and X = Cl, Br, and I. *J. Phys. Chem. C* **2018**, *122*, 158−170.
(18) Jain, A.; Voznyy, O.; Sargent, E. H. High-Throughput Screening of Lead-Free Perovskite-Like Materials for Optoelectronic Applications. *J. Phys. Chem. C* **2017**, *121*, 7183−7187.
(19) McClure, E. T.; Ball, M. R.; Windl, W.; Woodward, P. M. Cs_2AgBiX_6 (X = Br, Cl): New Visible Light Absorbing, Lead-Free Halide Perovskite Semiconductors. *Chem. Mater.* **2016**, *28*, 1348−1354.
(20) Volonakis, G.; Haghighirad, A. A.; Milot, R. L.; Sio, W. H.; Filip, M. R.; Wenger, B.; Johnston, M. B.; Herz, L. M.; Snaith, H. J.; Giustino, F. $Cs_2InAgCl_6$: A New Lead-Free Halide Double Perovskite with Direct Band Gap. *J. Phys. Chem. Lett.* **2017**, *8*, 772−778.
(21) Wei, F.; Deng, Z.; Sun, S.; Zhang, F.; Evans, D. M.; Kieslich, G.; Tominaka, S.; Carpenter, M. A.; Zhang, J.; Bristowe, P. D.; Cheetham, A. K. Synthesis and Properties of a Lead-Free Hybrid Double Perovskite: $(CH_3NH_3)_2AgBiBr_6$. *Chem. Mater.* **2017**, *29*, 1089−1094.
(22) Creutz, S. E.; Crites, E. N.; De Siena, M. C.; Gamelin, D. R. Colloidal Nanocrystals of Lead-Free Double-Perovskite (Elpasolite) Semiconductors: Synthesis and Anion Exchange to Access New Materials. *Nano Lett.* **2018**, *18*, 1118−1123.
(23) Gao, W.; Ran, C.; Xi, J.; Jiao, B.; Zhang, W.; Wu, M.; Hou, X.; Wu, Z. High-Quality $Cs_2AgBiBr_6$ Double Perovskite Film for Lead-Free Inverted Planar Heterojunction Solar Cells with 2.2% Efficiency. *Chem. Phys. Chem.* **2018**, *19*, 1696−1700.
(24) Locardi, F.; Cirignano, M.; Baranov, D.; Dang, Z.; Prato, M.; Drago, F.; Ferretti, M.; Pinchetti, V.; Fanciulli, M.; Brovelli, S.; De Trizio, L.; Manna, L. Colloidal Synthesis of Double Perovskite $Cs_2AgInCl_6$ and Mn-Doped $Cs_2AgInCl_6$ Nanocrystals. *J. Am. Chem. Soc.* **2018**, *140*, 12989−12995.
(25) Arfin, H.; Kaur, J.; Sheikh, T.; Chakraborty, S.; Nag, A. Bi^{3+}-Er^{3+} and Bi^{3+}-Yb^{3+} Codoped $Cs_2AgInCl_6$ Double Perovskite Near Infrared Emitters. *Angew. Chem., Int. Ed.* **2020**, *59*, 1−6.
(26) Lee, W.; Hong, S.; Kim, S. Colloidal Synthesis of Lead-Free Silver−Indium Double-Perovskite $Cs_2AgInCl_6$ Nanocrystals and Their Doping with Lanthanide Ions. *J. Phys. Chem. C* **2019**, *123*, 2665−2672.
(27) Liu, Y.; Jing, Y.; Zhao, J.; Liu, Q.; Xia, Z. Design Optimization of Lead-Free Perovskite $Cs_2AgInCl_6$:Bi Nanocrystals with 11. 4% Photoluminescence Quantum Yield. *Chem. Mater.* **2019**, *31*, 3333−3339.
(28) Zhao, F.; Song, Z.; Zhao, J.; Liu, Q. Double Perovskite $Cs_2AgInCl_6$:Cr^{3+}: Broadband and Near-Infrared Luminescent Materials. *Inorg. Chem. Front.* **2019**, *6*, 3621−3628.
(29) Slavney, A. H.; Leppert, L.; Bartesaghi, D.; Gold-Parker, A.; Toney, M. F.; Savenije, T. J.; Neaton, J. B.; Karunadasa, H. I. Defect-Induced Band-Edge Reconstruction of a Bismuth-Halide Double Perovskite for Visible-Light Absorption. *J. Am. Chem. Soc.* **2017**, *139*, 5015−5018.
(30) Karmakar, A.; Dodd, M. S.; Agnihotri, S.; Ravera, E.; Michaelis, V. K. Cu(II)-Doped $Cs_2SbAgCl_6$ Double Perovskite: A Lead-Free, Low-Bandgap Material. *Chem. Mater.* **2018**, *30*, 8280−8290.
(31) Choudhury, B.; Dey, M.; Choudhury, A. Defect Generation, d-d Transition, and Band Gap Reduction in Cu-Doped TiO_2 Nanoparticles. *Int. Nano Lett.* **2013**, *3*, 25.
(32) De, A.; Mondal, N.; Samanta, A. Luminescence Tuning and Exciton Dynamics of Mn-Doped $CsPbCl_3$ Nanocrystals. *Nanoscale* **2017**, *9*, 16722−16727.
(33) Hills-Kimball, K.; Pérez, M. J.; Nagaoka, Y.; Cai, T.; Yang, H.; Davis, A. H.; Zheng, W.; Chen, O. Ligand Engineering for Mn^{2+} Doping Control in $CsPbCl_3$ Perovskite Nanocrystals via a Quasi-Solid−Solid Cation Exchange Reaction. *Chem. Mater.* **2020**, *32*, 2489−2500.
(34) Imran, M.; Caligiuri, V.; Wang, M.; Goldoni, L.; Prato, M.; Krahne, R.; De Trizio, L.; Manna, L. Benzoyl Halides as Alternative Precursors for the Colloidal Synthesis of Lead-Based Halide Perovskite Nanocrystals. *J. Am. Chem. Soc.* **2018**, *140*, 2656−2664.
(35) Liao, Q.; Chen, J.; Zhou, J.; Wei, T.; Zhang, L.; Chen, D.; Huang, F.; Pang, Q.; Zhang, J. Z. Bandgap Engineering of Lead-Free Double Perovskite $Cs_2AgInCl_6$ Nanocrystals via Cu^{2+}-Doping. *J. Phys. Chem. Lett.* **2020**, *11*, 8392−8398.
(36) Ji, F.; Huang, Y.; Wang, F.; Kobera, L.; Xie, F.; Klarbring, J.; Abbrent, S.; Brus, J.; Yin, C.; Simak, S. I.; Abrikosov, I. A.; Buyanova, I. A.; Chen, W. M.; Gao, F. Near-Infrared Light-Responsive Cu-Doped $Cs_2AgBiBr_6$. *Adv. Funct. Mater.* **2020**, *30*, 2005521.
(37) Yao, M.-M.; Wang, L.; Yao, J.-S.; Wang, K.-H.; Chen, C.; Zhu, B.-S.; Yang, J.-N.; Wang, J.-J.; Xu, W.-P.; Zhang, Q.; Yao, H.-B. Improving Lead-Free Double Perovskite $Cs_2NaBiCl_6$ Nanocrystal Optical Properties via Ion Doping. *Adv. Optical Mater.* **2020**, *8*, 1901919.
(38) Xiao, Z.; Du, K.-Z.; Meng, W.; Mitzi, D. B.; Yan, Y. Chemical Origin of the Stability Difference between Copper(I)- and Silver(I)-Based Halide Double Perovskites. *Angew. Chem., Int. Ed.* **2017**, *56*, 12107−12111.
(39) Luo, J.; Wang, X.; Li, S.; Liu, J.; Guo, Y.; Niu, G.; Yao, L.; Fu, Y.; Gao, L.; Dong, Q.; Zhao, C.; Leng, M.; Ma, F.; Liang, W.; Wang, L.; Jin, S.; Han, J.; Zhang, L.; Etheridge, J.; Wang, J.; Yan, Y.; Sargent, E. H.; Tang, J. Efficient and Stable Emission of Warm-white Light from Lead-free Halide Double Perovskites. *Nature* **2018**, *563*, 541−545.
(40) Choudhury, B.; Dey, M.; Choudhury, A. Shallow and Deep Trap Emission and Luminescence Quenching of TiO_2 Nanoparticles on Cu Doping. *Appl. Nanosci.* **2014**, *4*, 499−506.

https://doi.org/10.1021/acsomega.1c03290
ACS Omega 2021, 6, 26952−26958